Electronic Supplementary Material (ESI) for Lab on a Chip.

DOI: 10.1039/D0LC00840K

Supplementary Material to:

Single-cell microfluidic impedance cytometry: from raw signals to cell phenotypes using data analytics

Carlos Honrado,[a] Paolo Bisegna,[b] Nathan S. Swami *[a] and Federica Caselli *[b]

[a] *Department of Electrical and Computer Engineering, University of Virginia, Charlottesville, VA 22904, USA.*
[b] *Department of Civil Engineering and Computer Science, University of Rome Tor Vergata, Via del Politecnico 1, 00133 Rome, Italy.*

S1. From multi-frequency impedance signals to cell dielectric parameters.

Impedance cytometry measurements typically involve cells suspended in a conductive medium. When measurements at multiple frequencies are performed, impedance spectra are obtained. These spectra critically depend on cell dielectric properties, and thus could be used to extract the latter from the former. To this aim, Maxwell's mixture theory (MMT) in conjunction with shell-models is typically used, by fitting simulated impedance spectra to measured ones (*e.g.* refs.[1,2]). However, measured impedance spectra depend not only on cell dielectric properties, but also on details of the measurement system, thus making the extraction process somewhat involved, as detailed below.

Using the typical differential measurement scheme (see Scheme 2A of the main text), the peak value of the measured signal S is given by the peak differential current I_{diff} multiplied by the transfer function of the acquisition system $H(\omega)$:

$$S = H(\omega) I_{diff} \tag{1}$$

where ω is the angular frequency. In turn, I_{diff} is given by:

$$I_{diff} = \frac{V_{appl}}{2Z_{dl}+Z_{med}} - \frac{V_{appl}}{2Z_{dl}+Z_{mix}} \cong V_{appl} \frac{(Z_{mix}-Z_{med})}{(2Z_{dl}+Z_{med})^2} \tag{2}$$

where V_{appl} is the applied voltage, Z_{dl} is the impedance associated with the electrode double layer capacitance, Z_{med} and Z_{mix} denote the impedances associated with medium-filled channel and channel with a suspended cell, respectively, which can be written as:

$$\tilde{Z}_{mix} = \frac{1}{j\,\omega\,\tilde{\varepsilon}_{mix}\,G} \quad , \qquad \tilde{Z}_{med} = \frac{1}{j\,\omega\,\tilde{\varepsilon}_{med}\,G} \tag{3}$$

Here $j^2 = -1$, G is the geometric constant of the system, and $\tilde{\varepsilon}_{mix}$ and $\tilde{\varepsilon}_{med}$ are the complex permittivities of the mixture and the medium, respectively, given by

$$\tilde{\varepsilon}_{mix} = \tilde{\varepsilon}_{med} \frac{1+2\varphi\tilde{f}_{CM}}{1-\varphi\tilde{f}_{CM}} \quad , \quad \tilde{\varepsilon}_{med} = \varepsilon_{med} + \sigma_{med}/j\omega \tag{4}$$

where ε_{med} and σ_{med} are the permittivity and conductivity of the suspending medium, φ is the volume ratio of the cell volume to the detection volume, and $\tilde{f}_{CM}$ is the Clausius-Mossotti factor of the mixture, which is given by:

$$\tilde{f}_{CM} = \frac{\tilde{\varepsilon}_{cell}-\tilde{\varepsilon}_{med}}{\tilde{\varepsilon}_{cell}+2\tilde{\varepsilon}_{med}} \tag{5}$$

where $\tilde{\varepsilon}_{cell}$ is the complex permittivity of the cell, which incorporates all the key information regarding the cell dielectric properties.

Under the assumption of small volume fraction (i.e., $\varphi \ll 1$), substituting eqs. (2)-(4) in eq. (1) results in:

$$S \cong -H(\omega)\frac{V_{appl}}{Z_{med}}\frac{1}{[1+(2Z_{dl}/Z_{med})]^2}3\varphi\tilde{f}_{CM} \qquad (6)$$

Eq. (6) proves that the measured signal S approximately linearly depends on φ, conveying information on cell size, and $\tilde{f}_{CM}$, conveying information on cell dielectric properties. However, S also depends on details of the measurement system (e.g., transfer function, applied voltage, double-layer impedance, medium properties).

The task of extracting φ and $\tilde{f}_{CM}$ from the measured signal S is usually accomplished by using reference beads. Denoting by S^{cell} and S^{bead} the signals respectively recorded under cell or reference-bead passage, Eq. (6) yields:

$$\frac{S^{cell}}{S^{bead}} = \frac{\tilde{f}_{CM}^{cell}\varphi^{cell}}{\tilde{f}_{CM}^{bead}\varphi^{bead}} = \frac{\tilde{f}_{CM}^{cell}}{\tilde{f}_{CM}^{bead}}\left(\frac{r^{cell}}{r^{bead}}\right)^3 \qquad (7)$$

where, assuming the cell is spherical, r^{cell} and r^{bead} respectively denote cell and bead radii. It is important to point out that details of the measurement system have been effectively cancelled out. Eq. (7) is then usually recast as:

$$\tilde{f}_{CM}^{cell}\left(\frac{r^{cell}}{r^{bead}}\right)^3 = \tilde{f}_{CM}^{bead}\frac{S^{cell}}{S^{bead}} \qquad (8)$$

Here $\tilde{f}_{CM}^{bead}$ and r^{bead}, relevant to reference beads, can be regarded as known quantities, whereas $\tilde{f}_{CM}^{cell}$ and r^{cell} are to be determined. The cell radius r^{cell} is usually determined using measurements at low-frequency, where the cell behaves like an insulating particle due to the presence of the plasma membrane, so that the Clausius-Mossotti factors $\tilde{f}_{CM}^{cell}$ and $\tilde{f}_{CM}^{bead}$ in Eq. (8) approximately cancel out, yielding:

$$\left(\frac{r^{cell}}{r^{bead}}\right)^3 = \frac{S^{cell@low\ freq}}{S^{bead@low\ freq}} \qquad (9)$$

After computing r^{cell} from Eq. (9), Eq. (8) can be recast as:

$$\tilde{f}_{CM}^{cell} = \tilde{f}_{CM}^{bead}\left(\frac{r^{bead}}{r^{cell}}\right)^3\frac{S^{cell}}{S^{bead}} \qquad (10)$$

emphasizing the linear relationship between $\tilde{f}_{CM}^{cell}$ and the measured signal S^{cell}. In fact, $\tilde{f}_{CM}^{cell}$ can be regarded as a *normalized signal*, conveying information on cell dielectric properties.

It remains to extract cell dielectric properties from the spectrum of $\tilde{f}_{CM}^{cell}$, as supplied in Eq. (10) by a simple normalization of the measured spectrum S^{cell}. The most typical method employed to extract cell dielectric properties from $\tilde{f}_{CM}^{cell}$ relies on standard shell-models[3–5], providing modelled data to be fitted to the spectrum of collected experimental data on $\tilde{f}_{CM}^{cell}$. While cells have an intricate internal structure surrounded by a membrane, a simplified approximation can be used based on single-shell or multi-shell models, wherein a cell is described as one or a series of ***n*** concentric shells with defined dielectric properties. Accordingly, the modelled $\tilde{f}_{CM}^{cell}$ is obtained by Eq. (5), whereby $\tilde{\varepsilon}_{cell}$ is an aggregation of the complex permittivities of all the ***n*** shells modelled. As an example, for the case of single-shell model, it can be computed as[6]:

$$\tilde{\varepsilon}_{cell} = \tilde{\varepsilon}_{mem}\frac{\gamma^3+2\left(\frac{\tilde{\varepsilon}_{int}-\tilde{\varepsilon}_{mem}}{\tilde{\varepsilon}_{int}+2\tilde{\varepsilon}_{mem}}\right)}{\gamma^3-\left(\frac{\tilde{\varepsilon}_{int}-\tilde{\varepsilon}_{mem}}{\tilde{\varepsilon}_{int}+2\tilde{\varepsilon}_{mem}}\right)}, \quad \gamma = \frac{r+d_{mem}}{r} \qquad (11)$$

where $\tilde{\varepsilon}_{mem}$ and $\tilde{\varepsilon}_{int}$ are the complex permittivities of the membrane and of the intracellular space, respectively, d_{mem} is the membrane thickness, and r is the cell radius. Under the assumption $d_{mem} \ll r$ it simplifies to:

$$\tilde{\varepsilon}_{cell} \cong \tilde{\varepsilon}_{int}\frac{\chi}{1+\chi}, \qquad \chi = \frac{\tilde{\varepsilon}_{mem}/d_{mem}}{\tilde{\varepsilon}_{int}/r} \qquad (13)$$

The complex permittivities of each specific component can in turn be calculated using:

$$\tilde{\varepsilon}_{mem} = \varepsilon_{mem} + \sigma_{mem}/j\omega, \;\; \tilde{\varepsilon}_{int} = \varepsilon_{int} + \sigma_{int}/j\omega \quad (14)$$

where ε and σ are modelled permittivities and conductivities for each component of the shell-model. In the simplified case of neglecting medium and intracellular permittivities, as well as membrane conductivity (i.e., $\varepsilon_{med} = \varepsilon_{int} = 0$, $\sigma_{mem} = 0$), $\tilde{f}_{CM}$ obeys a Debye relaxation:

$$\tilde{f}_{CM} = f_{CM.\infty} + \frac{f_{CM.0} - f_{CM.\infty}}{1 + j\omega\tau} \quad (15)$$

where

$$f_{CM,\infty} = \frac{\sigma_{int} - \sigma_{med}}{\sigma_{int} + 2\sigma_{med}}, \;\; f_{CM,0} = -\frac{1}{2}, \;\; \tau = \frac{r\varepsilon_{mem}}{d_{mem}}\left(\frac{1}{\sigma_{int}} + \frac{1}{2\sigma_{med}}\right) \quad (16)$$

These simplified formulas show that the features of the experimental spectrum of $\tilde{f}_{CM}$ convey information on cell constituents: e.g., the high-frequency behaviour is related to the intracellular conductivity, whereas the relaxation frequency $1/(2\pi\tau)$ conveys information on membrane properties.

In the general case, the modelled permittivities and conductivities can be comprised of a range of values which will be iterated by the fitting algorithm. This fitting process relies on the acquisition of data at a wide frequency range, so that the different cellular components probed at each frequency region can provide information about the overall mixture. The developed models are then iterated in order to identify the specific combination of dielectric parameters which give an optimal fit to the data. The specific fitting process implemented (e.g. least mean squares) can be developed based on the computational tools available.

Effectively, a series of modelled $\tilde{f}_{CM}$ values are calculated based on iterative dielectric properties. A common practice is to calculate the Real ($\Re(\tilde{f}_{CM})$) and Imaginary ($\Im(\tilde{f}_{CM})$) parts of the Clausius-Mossotti factor, and to generate the corresponding relaxation curves. Both population-based spectra[1] (Fig. S1A) and single-cell spectra[2] (Fig. S1B) have been presented in the literature. By fitting each curve to the Real and Imaginary parts of the experimental impedance data and obtaining the optimal fit, the dielectric properties of the particle can be estimated (Fig. S1).

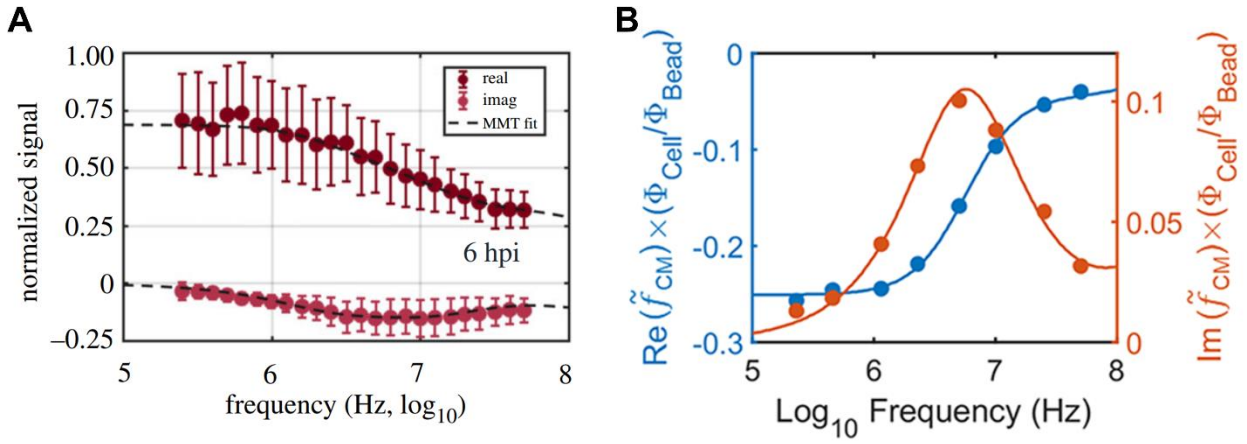

Fig. S1 – Multi-shell model fitting to experimental data of (A) malaria parasite infected-RBCs and (B) a ghost RBC for both the Real and Imaginary parts of the mixture impedance. Images were adapted with permission from (A) ref. [1], copyright 2018 The Royal Society; and (B) ref. [2], copyright 2020 American Chemical Society.

S2. Comparison of modelling approaches used in microfluidic impedance cytometry

Table S1: Comparison of the three modeling approaches (cf. Section 3.2 of the main text and Refs.[7,8])

Modelling approach	Advantages	Disadvantages	Main application
Maxwell's mixture theory (MMT)	Closed form description of cell polarization in electric fields; Useful to understand the physics behind the experimental phenomenon; Low computational cost.	Limited to: low volume fraction; spherical/ellipsoidal particles and associated single/multi shell models; quasi-homogeneous fields distribution (i.e., cell centred between electrodes).	It is the standard approach to compute cell dielectric properties by fitting simulated impedance spectra to measured ones.
Equivalent circuit models	Easy to understand from an electrical engineer point of view; Low computational cost; Easily integrated with circuit analysis software to simulate the whole measurement system.	Not direct link with cell intrinsic biophysical properties; Such link requires introducing further modelling (e.g., MMT and shell-models), thus inheriting their limitations.	Useful for measurement system optimization (e.g., to find the optimal frequency to achieve the maximum measurement sensitivity).
Finite element method	The analysis can be performed for any channel/cell geometry and dielectric structure, and for any cell position in the channel. Therefore, the impedance trace recorded as the cell flows through the device can be simulated.	High computational cost to obtain accurate results; Need for suitably designed meshes; Long simulation times.	It is a powerful tool for in-silico chip design and optimization; Simulated impedance traces are useful to interpret the experimental ones and can be used to test signal-processing routines.

S3. An approach for high-throughput quantification of bioelectrical markers (Zhang *et al.*[9])

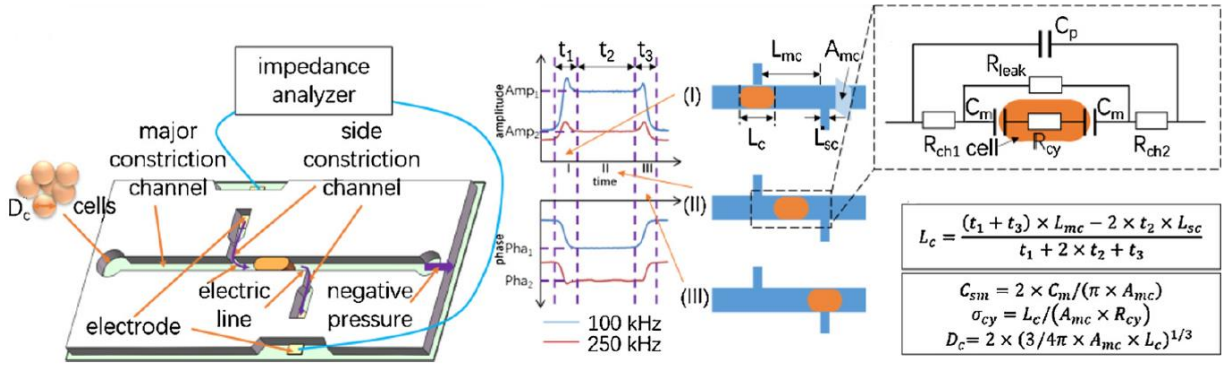

Fig. S2: Microfluidic platform and associated equivalent circuit model developed by Zhang *et al*. [9]. The equivalent circuit model is used to quantify single-cell intrinsic bioelectrical markers (specific membrane capacitance C_{sm}, cytoplasm conductivity σ_{cy} and cell diameter of D_c) by using the electrical features extracted from the impedance amplitude and phase waveforms at two frequencies (100 kHz and 250 kHz), along with geometrical parameters of the constriction channel. Reprinted with permission form ref. [9], copyright 2020 Elsevier B.V..

S4. Machine learning-based analysis of impedance cytometry data

Table S2: Survey of recent works using machine learning to analyze impedance cytometry data streams or impedance-based cell features (RNN: Recurrent Neural Network; bi-LSTM: bidirectional long short-term memory; FEM: Finite Element Method; RMSE: root mean squared error). For an introduction to the basic glossary and concepts of machine learning in microfluidics the Reader is referred to *e.g.* Riordon *et al.*[10].

Neural-networks for processing of impedance cytometry data streams				
Application	**Network type**	**Data set**	**Results**	**Ref.**
Real-time processing of impedance cytometry data streams.	Regression RNN with 4 layers (input, bi-LSTM, fully connected, regression). The bi-LSTM layer has one hundred hidden units and uses a hyperbolic tangent activation function.	Synthetic (FEM) datasets (known target features); Experimental datasets relevant to beads (5,6, and 7 µm diameter), yeasts, RBCs. Target features are obtained with a template-fitting approach.	Prediction of cell/particle diameter, velocity and position; RMSE of predicted values with respect to target values (bead mixture): 0.09 µm (diameter), 2.2% (velocity), 2.4% (position). Unit prediction time below 0.4 ms.	Honrado *et al.* 2020[11]
Pattern recognition in signal waveforms from a Coulter sensor network, including interference patterns.	Region Proposal Network (RPN) followed by Sensor Classification Network (SCN). They are Convolutional Neural Networks (CNN), with several layers including: convolutional layers, rectified linear units (ReLU), pooling layers and fully connected layers.	Experimental data from human ovarian, breast and prostate cell lines. Data augmentation based on power and duration scaling. Correlation-based labelling of the signal waveform. Benchmarking against optical images.	Prediction of size, velocity and location of each particle detected. Recognition of interference patterns of Coulter sensor waveforms to resolve data from coincidence particles. Unit prediction time 0.61 ms (RPN) and 0.67 ms (SCN).	Wang *et al.* 2019[12]
Fast coincidence resolution for increased throughput.	Classification RNN with 5 layers (input, bi-LSTM, fully connected, softmax, classification) followed by Regression RNN with 4 layers (input, bi-LSTM, fully connected, regression).	Synthetic (FEM) datasets (known target features); Artificial dataset created by superposition of single-particle events.	Prediction of event class: singlet, doublet, triplet, quadruplet; Prediction of single-particle event features (amplitude, width, transit time).	Caselli *et al.* 2020[13]
Machine learning for feature-based population clustering				
Application	**Network type/Approach**	**Data set**	**Results**	**Ref.**
Pattern recognition to classify cell types based on characteristic dielectric properties of single cells	Feed forward neural network with 2 layers (hidden and output), and with sigmoid hidden and softmax output neurons. A loop function was used to enumerate the hidden neuron number to avoid inappropriate selections of neuron numbers.	Estimated dielectric properties data from lung cancer cell lines A549 & H1299; Data was divided into training (70%), validation (15%) and testing (15%) subsets.	Cell classification success rates of 89.1% when using C_{sm} alone, 81.2% when using σ_{cy} alone and 90.9% when taking in consideration both dielectric properties, were obtained between H1299 and HeLa cells. Cell classification success rates of 71.7% when using C_{sm} alone, 74.2% when using σ_{cy} alone and 76.5% when taking in consideration both dielectric properties, were obtained between A549 and EMT-activated A549.	Zhao *et al.* 2018[14]
Classification of cell types based on measured impedance and deformability parameters of single cells	Back propagation neural network with 3 layers (input, hidden and output) and a sigmoid activation function.	Measured impedance and deformability data of MCF-7 cells; Data was divided into training (70%), validation (15%) and testing (15%) subsets.	Cell classification success rates of 87.8% when using impedance alone, 70.1% when using total transit-time alone, 42.7% when using relaxation index alone and 93.3% when taking in consideration impedance, transit-time and relaxation index were obtained between MCF-7 cells with different drug treatments.	Yang *et al.* 2019[15]
Prediction of cell viability based on measured impedance data of single cells	Support vector machines for classification and regression with a Gaussian Kernel for calculation of the Euclidian distance squared between two feature vectors, and a 8-feature matrix (impedance data at 4 different frequencies).	Measured impedance data of T47D cells; Training dataset comprised of 3 different tumor cell test samples of varying viability (90% live, 50% live and 82% live)	Viability classification of cells using impedance magnitude and phase data at 500 kHz, 20 MHz, 25 MHz and 30 MHz resulted in a confusion matrix with a classifier accuracy of 95.9%, a True Positive rate of 95% and a True Negative rate of 97%.	Ahuja *et al.* 2019[16]

References

1 C. Honrado, L. Ciuffreda, D. Spencer, L. Ranford-Cartwright and H. Morgan, *J. R. Soc. Interface*, 2018, **15**, 20180416.

2 D. Spencer and H. Morgan, *ACS Sensors*, 2020, **5**, 423–430.

3 T. Hanai, N. Koizumi and A. Irimajiri, *Biophys. Struct. Mech.*, 1975, **1**, 285–294.

4 Y. Huang, R. Hölzel, R. Pethig and X. B. Wang, *Phys. Med. Biol.*, 1992, **37**, 1499–1517.

5 A. Irimajiri, T. Hanai and A. Inouye, *J. Theor. Biol.*, 1979, **78**, 251–269.

6 P. R. C. Gascoyne, F. F. Becker and X. B. Wang, *Bioelectrochemistry Bioenerg.*, , DOI:10.1016/0302-4598(94)05015-M.

7 S. Gawad, K. Cheung, U. Seger, A. Bertsch and P. Renaud, *Lab Chip*, 2004, **4**, 241–251.

8 T. Sun, N. G. Green and H. Morgan, *NANO Br. Reports Rev.*, 2008, **3**, 55–63.

9 Y. Zhang, H. Liang, H. Tan, D. Chen, Y. Wang, Y. Xu, J. Wang and J. Chen, *Sensors Actuators, B Chem.*, 2020, **317**, 128231.

10 J. Riordon, D. Sovilj, S. Sanner, D. Sinton and E. W. K. Young, *Trends Biotechnol.*, 2019, **37**, 310–324.

11 C. Honrado, J. S. McGrath, R. Reale, P. Bisegna, N. S. Swami and F. Caselli, *Anal. Bioanal. Chem.*, 2020, **412**, 3835–3845.

12 N. Wang, R. Liu, N. Asmare, C. H. C. H. Chu and A. F. F. Sarioglu, *Lab Chip*, 2019, **19**, 3292–3304.

13 F. Caselli, A. De Ninno, R. Reale, L. Businaro and P. Bisegna, in *24nd International Conference on Miniaturized Systems for Chemistry and Life Sciences (MicroTAS 2020)*, 2020.

14 Y. Zhao, K. Wang, D. Chen, B. Fan, Y. Xu, Y. Ye, J. Wang, J. Chen and C. Huang, *Biosens. Bioelectron.*, 2018, **111**, 138–143.

15 D. Yang, Y. Zhou, Y. Zhou, J. Han and Y. Ai, *Biosens. Bioelectron.*, 2019, **133**, 16–23.

16 K. Ahuja, G. M. Rather, Z. Lin, J. Sui, P. Xie, T. Le, J. R. Bertino and M. Javanmard, *Microsystems Nanoeng.*, 2019, **5**, 34.